Materials Chemistry and Physics 247 (2020) 122854

Contents lists available at ScienceDirect

Materials Chemistry and Physics

journal homepage: www.elsevier.com/locate/matchemphys

Deposition and characterization of ZnO thin films on GaAs and Pt/GaAs substrates

Juliana Chawich [a,b], Sabina Kuprenaite [a], Samuel Margueron [a], Pascal Boulet [c], Jan J. Dubowski [b], Céline Elie-Caille [a], Thérèse Leblois [a,*]

[a] FEMTO-ST Institute - CNRS UMR-6174, Université de Bourgogne Franche-Comté, 15B Av. des Montboucons, 25030, Besançon, France
[b] Laboratoire Nanotechnologies Nanosystèmes (LN2), CNRS UMI-3463, Institut Interdisciplinaire d'Innovation Technologique (3IT), Université de Sherbrooke, 3000 Boulevard Université, Sherbrooke, J1K 0A5, Québec, Canada
[c] Jean Lamour Institute, CNRS UMR-7198, Université de Lorraine, 2 Allée André Guinier, 54011 Nancy, France

ARTICLE INFO

Keywords:
ZnO films
GaAs substrate
Platinum electrode
Buffer layer
Magnetron sputtering

ABSTRACT

This work reports the deposition and characterization of piezoelectric ZnO thin films on semi-insulating GaAs substrates for the fabrication of bulk acoustic waves sensors. ZnO films are deposited at 350 °C and low deposition rate using reactive radio frequency magnetron sputtering. The use of a Pt bottom electrode, between ZnO and GaAs, with and without Ti buffer layer, as well as the effect of the substrate crystallographic orientation are investigated. The characterization of the deposited films is performed to determine the optimal parameters for obtaining high-quality films and ZnO residual conductivity. ZnO films are textured along the c-axis for all GaAs cuts. The highest structural quality is obtained on (100) GaAs substrates. Moreover, the presence of the Ti buffer layer improves the texture quality, surface roughness and residual stresses. The lowest residual conductivity is determined for the ZnO/Pt/Ti/GaAs structure. However, a slight diffusion of Ga and Ti into Pt is observed, which may be of concern if Pt is used as a bottom electrode. Therefore, for thickness excitation functioning, further optimization of the Pt/GaAs interface has to be considered.

1. Introduction

Gallium arsenide is a III–V direct gap semiconductor presenting a combination of physical properties that made it widely used in microelectronics and opto-electronics devices [1]. The microfabrication of GaAs has been widely investigated for device miniaturization and integration [2,3]. In addition, semi-insulating GaAs combines advanced MEMS and piezoelectric properties required for sensor transducing [4]. Moreover, its surface can be functionalized and regenerated, constituting a real advantage for the development of reusable sensors [5–8]. Despite the many potential applications of this material, only a few GaAs based sensors have been developed, in spite of a significant amount of research work carried out [9,10]. In this context, we have previously designed and fabricated a resonant GaAs sensor operating in shear modes of bulk acoustic waves generated by lateral field excitation [11,12]. However, the major obstacles to the implementation of such sensor were the low piezoelectric sensitivity and environmental stability, resulting in poor performances of the device [13]. To overcome these drawbacks, our research has been oriented towards the enhancement of the piezoelectric coupling of the GaAs-based structure. ZnO thin films have been occasionally used for probing weak/non-piezoelectric GaAs crystal orientations [14–17]. The deposition of piezoelectric ZnO thin films on GaAs substrates could then potentially increase the electromechanical coupling of the transducer and is investigated in this paper.

ZnO is a semiconductor material with interesting physical properties that place it among the most used materials in micro and opto-electronics. Apart from its large direct bandgap, high electron mobility and strong room-temperature luminescence, ZnO has been renowned as

* Corresponding author.
E-mail address: therese.leblois@femto-st.fr (T. Leblois).

https://doi.org/10.1016/j.matchemphys.2020.122854
Received 6 December 2019; Received in revised form 21 February 2020; Accepted 25 February 2020
Available online 27 February 2020

a very promising material for acoustic applications thanks to its high piezoelectric coefficients. Indeed, ZnO piezoelectric properties have been widely investigated [18–20] and applied for diverse applications in many fields [21,22]. More specifically, ZnO films have been used in surface and bulk acoustic wave devices for filtering and sensing applications [23–26], due to the numerous advantages that this material presents compared to other piezoelectric thin film materials such as AlN and PZT [27]. For instance, good film crystallinity and control of the stoichiometry of a ZnO thin film and its texture can be easily achieved at relatively low deposition temperatures [28]. In addition, ZnO normally has a low film stress and a relatively good adhesion with most substrates. Furthermore, ZnO material is considered as biosafe and therefore is suitable for biomedical and microfluidic applications [29].

ZnO thin films have been deposited using a large variety of growth methods due to the diversity of its applications [30–32]. However, obtaining ZnO films of high crystalline quality usually requires the use of high deposition temperature and very low growth rates. The sputtering technique is then preferred, mainly because of its low thermal budget, the control of the deposition parameters, the interfacial adhesion to the substrate and the high reproducibility [33–35].

The growth and characterization of ZnO films have been widely reported on different kinds of substrates [36–40]. However, there are only few reports on the growth on GaAs substrates [41–44]. The oxidation of GaAs and interdiffusion of ZnO at high deposition temperatures (>400 °C) are to be considered to avoid the degradation of the film resistivity or the unwanted doping of GaAs during the sputtering process [45,46]. In addition, the oxidation of GaAs surfaces may prevent the growth of crystalline structures. To address this problem, several studies have been carried out and different buffer layers have been tested such as SiO_2 [41], Si_3N_4 [47], ZnS [48] and ZnSe [49]. However, none of these buffer layers met the structural and functional requirements of the film, especially for the fabrication of a bulk acoustic waves transducer.

In this work, the deposition of ZnO films on oriented GaAs substrates using reactive Radio Frequency (RF) magnetron sputtering is reported. The addition of Pt bottom electrode with Ti buffer layer is investigated. Little is known on the use of Pt for depositing piezoelectric ZnO films on GaAs substrates. The quality of the deposited films is studied using different characterization techniques. Based on these measurements, the effects of the substrate orientation and the use of the buffer layer on the film quality are evaluated.

2. Materials and methods

2.1. Deposition of ZnO thin films

ZnO thin films were deposited on GaAs substrates of different crystallographic orientations (100), (110), (111)A and (111)B, where A and B stand for Ga and As terminated surfaces respectively. The used substrates were semi-insulating and undoped GaAs wafers (supplied by AXT, Inc.) of 3 inches in diameter and 625 ± 25 μm in thickness (double-side polished). Two sets of depositions were carried out for each substrate orientation: the first is performed directly on the GaAs substrates, and the second is done using a Pt bottom electrode. The latter consisted of a 150 nm thick Pt metallic layer and a Ti buffer layer of 15 nm thickness, both deposited using cathodic sputtering. The deposition of ZnO films was carried out using reactive RF magnetron sputtering (Plassys MP450S) using metallic zinc target. Prior to deposition, the substrates were cleaned under a plasma of argon and oxygen for 2 min and the target was presputtered for 2 min to remove contaminants. The substrate temperature and the chamber pressure were set to 350 °C and 4 mTorr, respectively. The O_2/Ar gas ratio was 1.5, providing a deposition rate of approximately 2.77 nm/min. The deposition time was 240–280 min.

Table 1
Experimental SIMS parameters used to collect the depth profiles of the deposited ZnO thin films.

Apparatus			ION-TOF SIMS IV
Ionic courant			0.5 pA
Pulse			19.1 ns
Pressure			5.0×10^{-9} Torr
Charge neutralization			2.35 A
Spectroscopy	Source		Bi+
	Energy		25 kV
	Analyzed surface		50 μm × 50 μm
	Spectral resolution		128 x 128 pixels
	Mass resolution	H/Si	0.7 ns
		^{29}Si	M/ΔM > 8000
Profiles	Source		Cs+ and O_2+
	Energy		3.0 kV
	Pulverized surface		300 μm × 300 μm

2.2. ZnO films characterization

The phase composition and out of plane orientation of the deposited ZnO films were analyzed by means of X-ray diffraction (XRD) using a Bruker D8 Advance diffractometer with monochromatic radiation CuKα as the X-ray source (λ = 1.5405 Å). Rocking curves and φ-scans were measured using a Bruker D8 Discover diffractometer with CoKα radiation (λ = 1.79026 Å) to assess the texture quality of the films. The rocking curves were measured for the (0002)-ZnO reflection to determine the mosaicity of the c-axis orientation. The texture quality of the layers was evaluated from the full width at half maximum (FWHM) of the rocking curves fitted using a Voigt function.

Raman spectra of the deposited films were collected at room temperature using S&I MonoVista polarized Raman microspectrometer with a laser excitation of 532 nm. The reference spectra were obtained by measuring Z- oriented ZnO single crystals and GaAs of different crystalline orientations: (100), (110), (111)A and (111)B. For each sample, the parallel and cross polarization spectra were measured and noted according to Porto notation in reference to the ZnO layer orientation using XRD orientation. The Raman selection rules, the frequencies and the symmetries of the fundamental Raman modes of ZnO and GaAs can be found in Refs. [50–52].

The surface topography of the films was characterized using a Nanowizard III AFM (JPK Instruments, Germany) mounted on a Leica microscope (Z16 APOA). Imaging was performed in air using Nano World NPS-10C cantilevers made from silicon nitride with a stiffness of 0.32 N/m. AFM images were collected in contact mode, at a frequency of 0.5 lines/sec with a resolution of 512 by 512 pixels. Scans of different dimensions (100 × 100 μm^2 to 1 × 1 μm^2) were made in order to have a representative sampling of the surface.

Ellipsometric spectra were measured using the UVISEL spectroscopic ellipsometer (HORIBA Jobin Yvon) in the range of 0.73 eV and 4.75 eV, at an angle of 70°. In order to estimate the thicknesses and optical properties of the films, a model composed of a ZnO layer with the substrate measured before deposition was used (with top surface of Pt or GaAs). The layer model is the excitonic model of K. Sato et al. [53] with free parameters. These parameters were first optimized on ZnO single crystal. The routine of optimization of the model started by searching for the thickness with fix parameter of the layer model of ZnO, and in a second time, the film parameters were relaxed. The final results gave χ^2 below 1 and can be considered very good. More complex models taking into account the roughness or the buffer layer were tested but did not give realistic optical properties.

Secondary ions mass spectrometry (SIMS) depth profiles of the deposited ZnO films were done in interlaced mode on a 100 μs cycle. In this mode, the sputtering source was used to remove the analyzed material for 80 μs. During the remaining 20 μs of the cycle, the flood gun sent a pulse of low energy electrons to discharge the surface. The surface was then bombarded with the primary ions of Bi^+, and the emitted

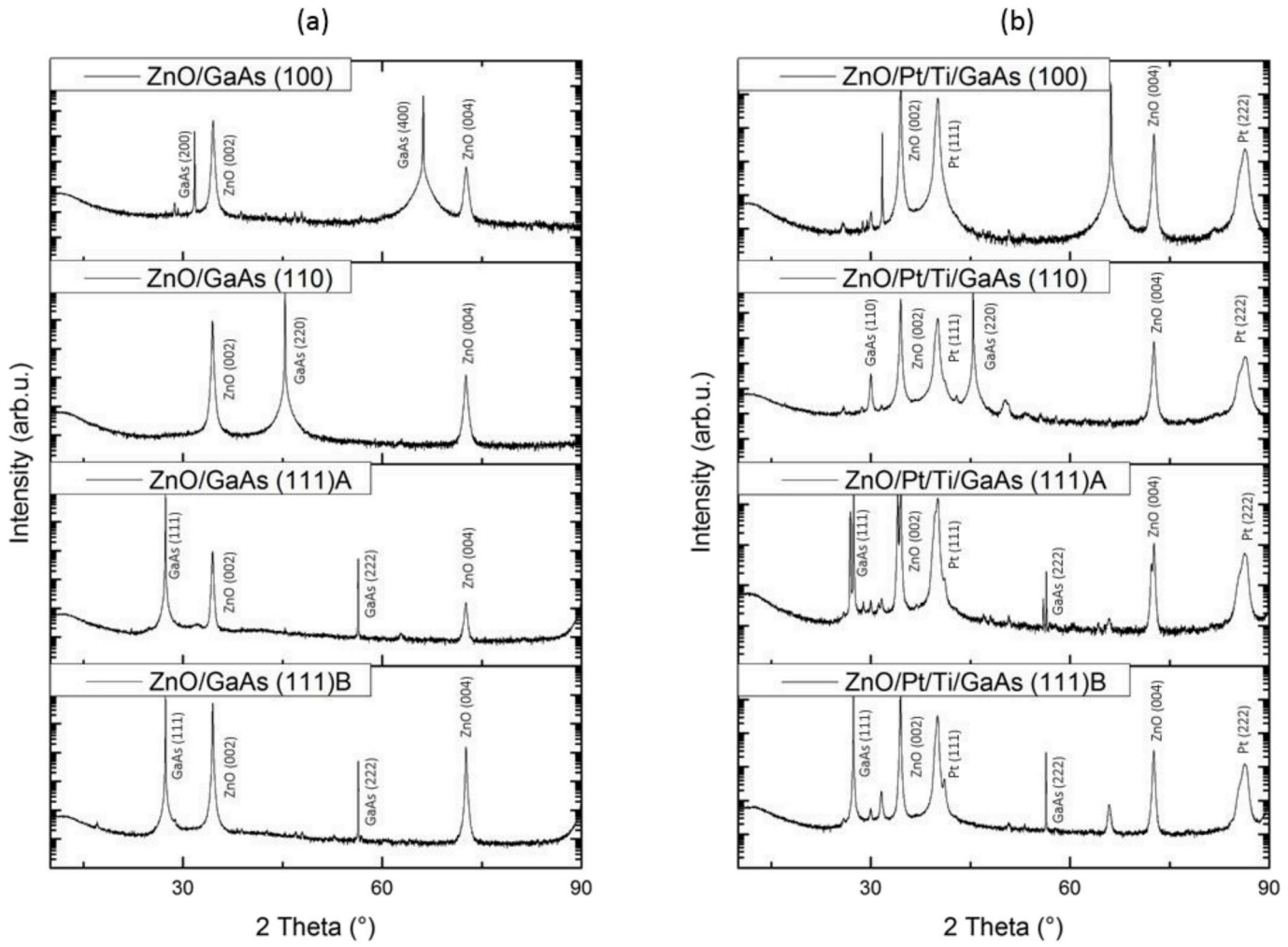

Fig. 1. θ/2θ X-ray diffraction patterns of ZnO films deposited on GaAs substrates with different crystallographic orientations without (a) and with (b) Pt/Ti buffer layer.

secondary ions were collected for analysis. The craters with dimensions of 300 μm × 300 μm were etched, and the analysis with the primary ions of Bi^+ was carried out in a region with dimensions of 50 μm × 50 μm located in the center of the crater to avoid the edge effect. All profiles were obtained to the interface of GaAs. The crater depth was then measured using a profilometer to determine the average erosion rate and to express the profiles as a function of the depth. A detailed list of the parameters used for this technique is provided in Table 1.

With regards to the elements expected in the present analysis, oxides, Pt, and As have a better detection yield of negative ions. On the other hand, Ti and Ga have a better yield of positive ions. Negative ion profiles were first established using a Cs^+ sputtering source to observe the profiles of ZnO, Pt, As and GaAs. Then, positive ion profiles were established using an O^{2+} sputtering source to observe the distribution of Zn, Ti, and Ga. Pt was also detected, but with a decreased intensity compared to what was found in negative ions profiles.

In plane conductivity was characterized by I(V) measurements using Keithley 2636B sourcemeter, at room temperature. Prior to the measurements, two electrodes made of chromium/gold (Cr 15 nm/Au 150 nm) and separated by a gap of 200 μm were deposited on top of the ZnO film to compare the residual conductivity of ZnO/GaAs and ZnO/Pt/GaAs structures.

3. Results and discussion

3.1. Structure and residual stresses

The XRD θ/2θ patterns of the ZnO films grown on differently oriented GaAs substrates with and without the Pt/Ti buffer layer are shown in Fig. 1. All XRD patterns show crystalline Würtzite structure with

Table 2
FWHM of (0002) ZnO rocking curve, c-lattice constant, strain and residual stress in ZnO thin films deposited on GaAs substrates with different crystallographic orientations with (+) and without (−) the Pt/Ti buffer bilayer.

GaAs orientation	(100)	(100)	(110)	(110)	(111)A	(111)A	(111)B	(111)B
Buffer bilayer	−	+	−	+	−	+	−	+
Rocking FWHM (° ± 0.25°)	5.2	1.42	–	1.55	5.5	1.47	5.84	1.48
c-lattice constant (Å ± 0.003 Å)	5.218	5.215	5.208	5.207	5.207	5.206	5.207	5.204
Strain (× 10^{-4})	25.0	19.0	6.3	3.8	3.7	1.2	3.7	1.3
Residual stress (MPa ±100 MPa) estimated from XRD data	−434	−332	−108	−65	−63	−21	−63	−22
Residual stress (MPa ±100 MPa) estimated from Raman data	−244	−57	−98	−59	−106	−49	−41	−21

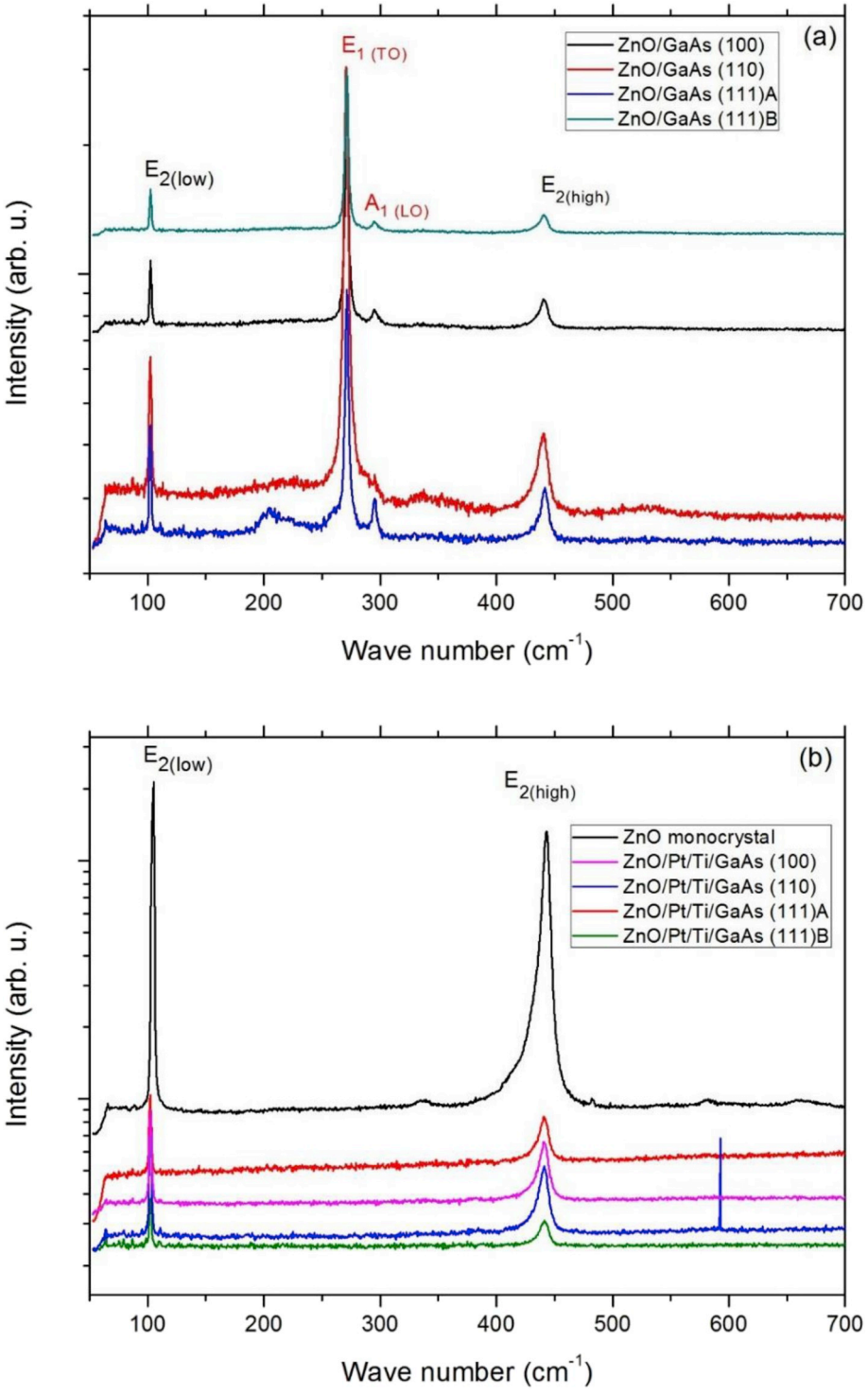

Fig. 2. Raman spectra collected in $Z(XY)\bar{Z}$ polarization configuration of ZnO films deposited on GaAs substrates with different crystallographic orientations without (a) and with (b) the Pt/Ti buffer bilayer. The GaAs modes are labelled in red. (For interpretation of the references to colour in this figure legend, the reader is referred to the Web version of this article.)

dominant reflections from the (000ℓ) ZnO planes. The reflections of other family planes were not observed for all substrates, confirming that the deposited layers were strongly textured along the c-axis of the hexagonal crystalline structure.

The mosaicity of the c-axis orientation was examined using rocking curve measurements of the 0002 ZnO reflection. ZnO films grown directly on GaAs presented a mosaicity ranging between 5.2° and 5.8°, represented by the FWHM of 0002 reflection rocking curve, while the films grown with a Pt/Ti buffer layer showed a mosaicity between 1.4° and 1.6° (Table 2). The texture quality was improved in the presence of the Pt/Ti buffer layer, making it independent of the used substrate cut. The direct growth of ZnO on GaAs substrates was influenced by the substrate surface orientation. The best texture quality was obtained on GaAs (100) surface (FWHM = 1.42°). The mosaicity was also high on GaAs (111) surfaces and similar for both of the surface terminations A (FWHM = 1.47°) and B (FWHM = 1.48°). The texture on GaAs (110) was

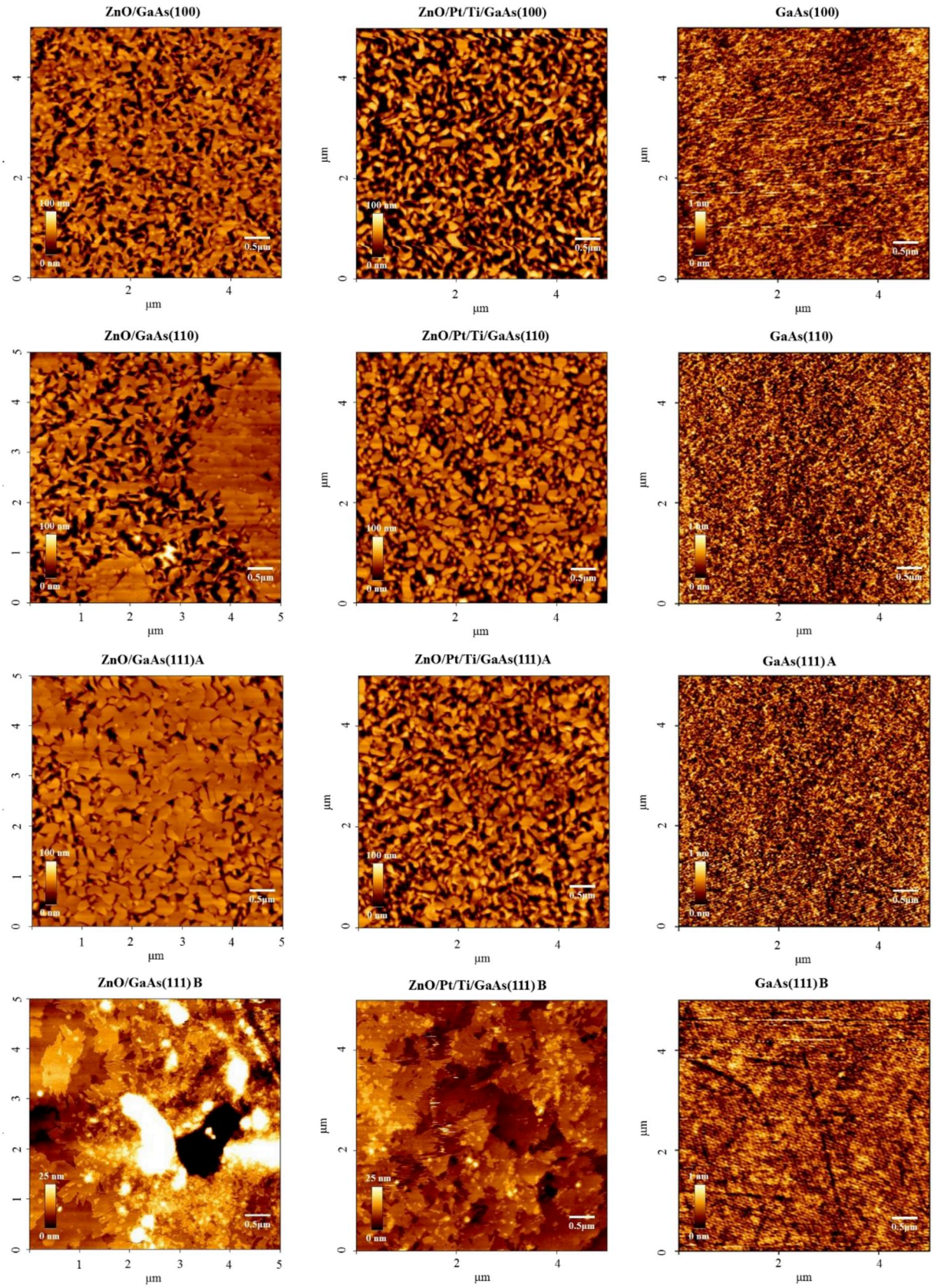

Fig. 3. AFM images of ZnO thin films deposited on GaAs substrates of different crystallographic orientations with and without the Pt/Ti buffer bilayer, and of GaAs bare surface of different cuts.

of slightly lower quality (FWHM = 1.55°). Furthermore, the films did not present any defined in-plane orientation with respect to the orientation of the substrate, for all GaAs cuts, as confirmed by the φ-scans of ZnO reflections.

The interplanar distance for the deposited ZnO films was calculated from the 2θ angle of the (0002)-plane reflection, after calibration of the θ/2θ pattern with respect to the reflections of the GaAs substrate (JCPDS data card No. 00-014-450). The calculated values of the c-lattice constant for each deposited film are reported in Table 2.

Compared with a ZnO single crystal lattice constant ($c_b = 5.2049$ Å), it is obvious that the ZnO films present slightly extended c-lattice parameters. Indeed, the shift of the diffraction reflection position from the bulk single-crystal value is mainly associated with thermal and intrinsic stresses produced within the film [54]. The 2θ position of the grown films is less than that of bulk single-crystal ZnO, indicating that the films are in a uniform state of stress with extended c-axis. The larger value of lattice constant for the grown films compared to the unstressed bulk single-crystal value shows that the unit cell is elongated along the c-axis, and compressive forces act in the plane of the film.

Indeed, the thermal stresses acting on the films are generated during the cooling process following the deposition of the ZnO films. The difference in the thermal expansion coefficients of the GaAs substrate and the deposited ZnO films results in the generation of stresses and consequently the deformation of the layer. The theoretical biaxial deformation ε_b related to the thermal stress can be determined from the relation:

$$\varepsilon_b = (\alpha_F - \alpha_S)\,(T_{dep} - T_a) \tag{1}$$

Where α_F and α_S represent the coefficients of thermal expansion of ZnO ($2.9 \times 10^{-6}\ K^{-1}$) and GaAs ($5.73 \times 10^{-6}\ K^{-1}$) respectively, T_{dep} is the temperature of the substrate during the deposition (350 °C) and T_a is the ambient temperature. Using ε_b, the theoretical values of the deformation ε_{zz} were determined using the equation:

$$\varepsilon_b = -\frac{C_{33}\varepsilon_{zz}}{2\ C_{13}} \tag{2}$$

The biaxial thermal stresses σ_b were determined using Hooke's law [55]:

$$\sigma_b = \left(C_{13} - \frac{(C_{11} + C_{12})\ C_{33}}{2C_{13}}\right)\varepsilon_{ZZ} \tag{3}$$

The calculated value of the theoretical thermal stress is - 208 MPa. The elastic constants of ZnO used in this calculation were: $C_{11} = 209.7 \pm 0.2$ GPa, $C_{12} = 121.1 \pm 0.3$ GPa, $C_{13} = 105.1 \pm 0.2$ GPa, $C_{33} = 210.9 \pm 0.1$ GPa [56].

Using XRD data, the strain ε_{zz} in the films was calculated from the shift of the 0002 ZnO reflection in the θ/2θ X-ray patterns, using the following equation [57]:

$$\varepsilon_{zz} = \frac{c_f - c_b}{c_b} \tag{4}$$

Where c_f is the lattice constant for the ZnO thin film and c_b is the lattice constant of bulk ZnO single crystal. The residual stress induced in the film was evaluated from the measured strain using equation (3).

The comparison of the residual stresses for the grown ZnO films shows that they are all subjected to compressive stresses (<500 MPa), which is consistent with the fact that the in-plane expansion coefficient of ZnO is lower than that of GaAs. Moreover, the films deposited on the Pt/Ti buffer layer show slightly lower stresses than the films deposited directly on GaAs. Although the thermal expansion of cubic GaAs is isotropic and all ZnO films presented the same crystallographic orientation, the highest residual stresses were developed in films grown on GaAs (100). The different stresses observed for the different cuts of GaAs could be explained by the argon ion pinning, which could generate additional intrinsic stresses adding to the thermal ones. The obtained values are in reasonable agreement with the theoretical thermal stress.

On the other hand, the Raman spectra obtained for ZnO thin films deposited directly on GaAs (Fig. 2a) clearly show the ZnO and GaAs Raman modes, whereas the spectra of ZnO films deposited on the Pt/Ti layer (Fig. 2b) show only the ZnO modes, due to the absorption by the Pt layer.

The polarization selection rules for Raman scattering in ZnO (Würtzite symmetry with 6 mm point group) predict that it is possible to identify the modes of the $E_{2(low)}$, $E_{2(high)}$ and $A_{1(LO)}$ modes in $Z(XX)\overline{Z}$ and $Z(YY)\overline{Z}$ polarization configurations, whereas for $Z(XY)\overline{Z}$ only the E_2 modes are observable. For the deposited ZnO films, the modes around 101 cm^{-1} and 437 cm^{-1} correspond to the $E_{2(low)}$ and $E_{2(high)}$ modes respectively, as predicted by the selection rules.

As for GaAs ($\overline{4}3$ m point group with zinc blende symmetry), it is possible to find the longitudinal modes $A_{1(LO)}$ for the planes (100) and (111) of GaAs, whereas this is not possible for the plane (110), and the transverse modes $E_{1(TO)}$ appear for the cuts (110) and (111) and not for (100) orientation. For GaAs, the spectra obtained for the various orientations confirm the stated selection rules of a blend cubic system. The $A_{1(LO)}$ and the $E_{1(TO)}$ modes are observable around 291 cm^{-1} and 267 cm^{-1} respectively.

The observed modes of ZnO films are slightly shifted from the wavenumbers of ZnO monocrystal. These Raman shifts can provide information on the state of the stresses acting on the ZnO layers. The wavenumber of the modes E under stress can be described as follows [58]:

$$\omega_E(TO) = a'\ E(TO)\ \left(\sigma_{xx} + \sigma_{yy}\right) + b'\ E(TO)\ \sigma_{zz} \pm \sqrt{c'_{E(TO)}\left(\sigma_{xx} - \sigma_{yy}\right)^2 + d'_{E(TO)}\left(\sigma_{xy}\right)^2} \tag{5}$$

Where σ_{xx}, σ_{yy} and σ_{zz} are the stresses along the axes X, Y and Z respectively (where Z is parallel to the c-axis, X- and Y-axis parallel to the a- and b-axis), $a'_{E(TO)}$, $b'_{E(TO)}$, $c'_{E(TO)}$ and $d'_{E(TO)}$ are the potential deformation constants expressed in terms of compliance.

The $c'_{E(TO)}$ is related to the division of $E_{(TO)}$ doubly degenerate. If the axes a and b are affected by the different constraints or if the plane ab is subjected to shear stresses, the mode $E_{(TO)}$ is divided into two components. However, the degeneration of $E_{(TO)}$ is usually quite weak and its division is difficult to identify, thus $c'_{E(TO)}$ is negligible. In addition, we assume that there are no shear stresses in the films, hence $\sigma_{xy} = 0$. The ZnO films, deposited on cubic substrates, are subjected to biaxial stresses σ_b in the plane of the substrate [58]. Thus, $\sigma_{xx} = \sigma_{yy} = \sigma_b$ and the shift of the modes $E_{(TO)}$ in the c-axis oriented planes can be expressed as:

$$\Delta\omega_{E\ (TO)} = 2\ a'_{E\ (TO)}\ \sigma_b \tag{6}$$

Where $a' = 1.4\ cm^{-1}$/GPa for the mode $E_{2(high)}$ (at 437 cm^{-1}) for ZnO. Thereby, the biaxial stresses σ_b can be calculated from the shift of the positions of the ZnO $E_{2(high)}$ modes wavenumbers:

$$\sigma_b = \frac{\Delta WE(TO)}{2a'\ E(TO)} \tag{7}$$

The values of stress, calculated from (7) for the different samples, are provided in Table 2. The low displacement of the $E_{2(High)}$ mode towards high frequencies is associated with compressive residual stresses. Moreover, the found values of the biaxial stresses are quite low (<0.25 GPa) and are close to the theoretical thermal stresses and to the stresses calculated from XRD data (see Table 2). The ZnO films grown on different cuts of GaAs directly or with Pt/Ti buffer layers presented comparable residual stress in the limits of the errors.

3.2. Surface morphology and roughness

Fig. 3 shows the atomic force microscopy (AFM) images of GaAs bare substrates and those of ZnO thin films deposited on them with and without the Pt/Ti buffer layer. The corresponding average roughness parameters (Rms) were determined using JPK software from several 5

Table 3
Average roughness parameters calculated from AFM images of GaAs substrates and ZnO thin films deposited on GaAs substrates of different crystallographic orientations with (+) and without (−) the buffer bilayer.

GaAs orientation	(100)	(100)	(110)	(110)	(111)A	(111)A	(111)B	(111)B
Rms for GaAs susbtrate (nm)	0.18 ± 0.03		0.21 ± 0.01		0.41 ± 0.03		0.17 ± 0.01	
Buffer bilayer	–	+	–	+	–	+	–	+
Rms for ZnO film (nm)	26.5 ± 1.8	17.9 ± 2.1	18.9 ± 2.3	17.4 ± 3.8	12.8 ± 1.8	10.8 ± 1.9	13.4 ± 7.7	2.7 ± 0.3

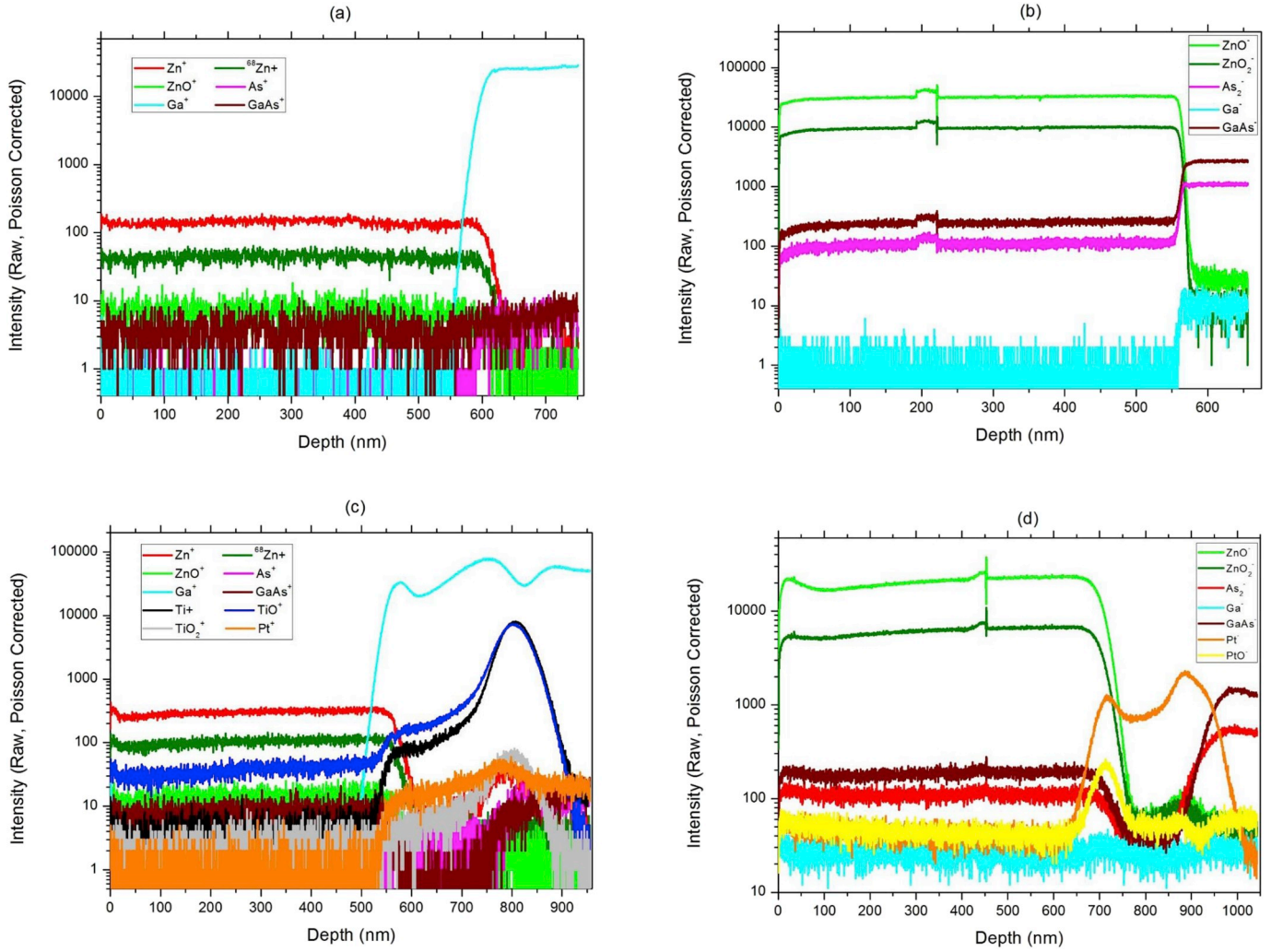

Fig. 4. Positive and negative ion depth profiles measured by SIMS in ZnO thin films grown on GaAs (100) (a, b), Pt/Ti/GaAs (100) (c, d), respectively.

μm × 5 μm^2 images (Table 3).

The dependence of the film morphology on the substrate's plane is shown on Fig. 3. The surface of the ZnO film deposited on GaAs (100) is the roughest, and the Rms decreases from 26.5 ± 1.8 nm to 17.9 ± 2.1 nm when the Pt/Ti layer is added. The films grown directly on GaAs (110) showed an inhomogeneous surface, with roughness parameters varying according to the organization of the crystallites. However, that is not the case when the Pt/Ti layer is added, since the grains distribution becomes more homogeneous. In the case of GaAs (111) substrates, although the surface roughness of the starting substrate is higher for GaAs (111)A than for GaAs (111)B, the surface of the ZnO thin film becomes more uniform on the Ga-terminated surface. Moreover, the roughness of the ZnO thin film changes between 13.4 ± 7.7 nm for direct growth and 2.7 ± 0.3 nm with the Pt/Ti layer for GaAs (111)B. The roughness parameters for all substrate orientations decrease in the presence of the buffer layer, indicating a better organization of the films. Hence, the presence of the buffer layer promotes the growth of a homogeneous crystalline structure by reducing surface heterogeneities.

Among the tested cuts, GaAs (100) has shown to promote the growth of high quality ZnO thin films, in terms of texture, flatness, homogeneity and roughness. Furthermore, the micromachining of resonant membranes in GaAs using chemical wet etching has been widely studied in our research group [2,3,9], and GaAs (100) has shown to produce promising and reproducible microstructures for sensing, which is not the case for the other cuts. Therefore, the GaAs (100) orientation will be selected for the rest of the study.

3.3. Layers interfaces and depth profiles

For a better understanding of the ZnO/buffer layer/GaAs structure, a physico-chemical analysis of the layers was conducted using SIMS. This allowed to obtain depth profiles of the elements distribution of the samples at the interfaces of the constituting layers (Fig. 4).

The examination of the depth profiles of ZnO films deposited on

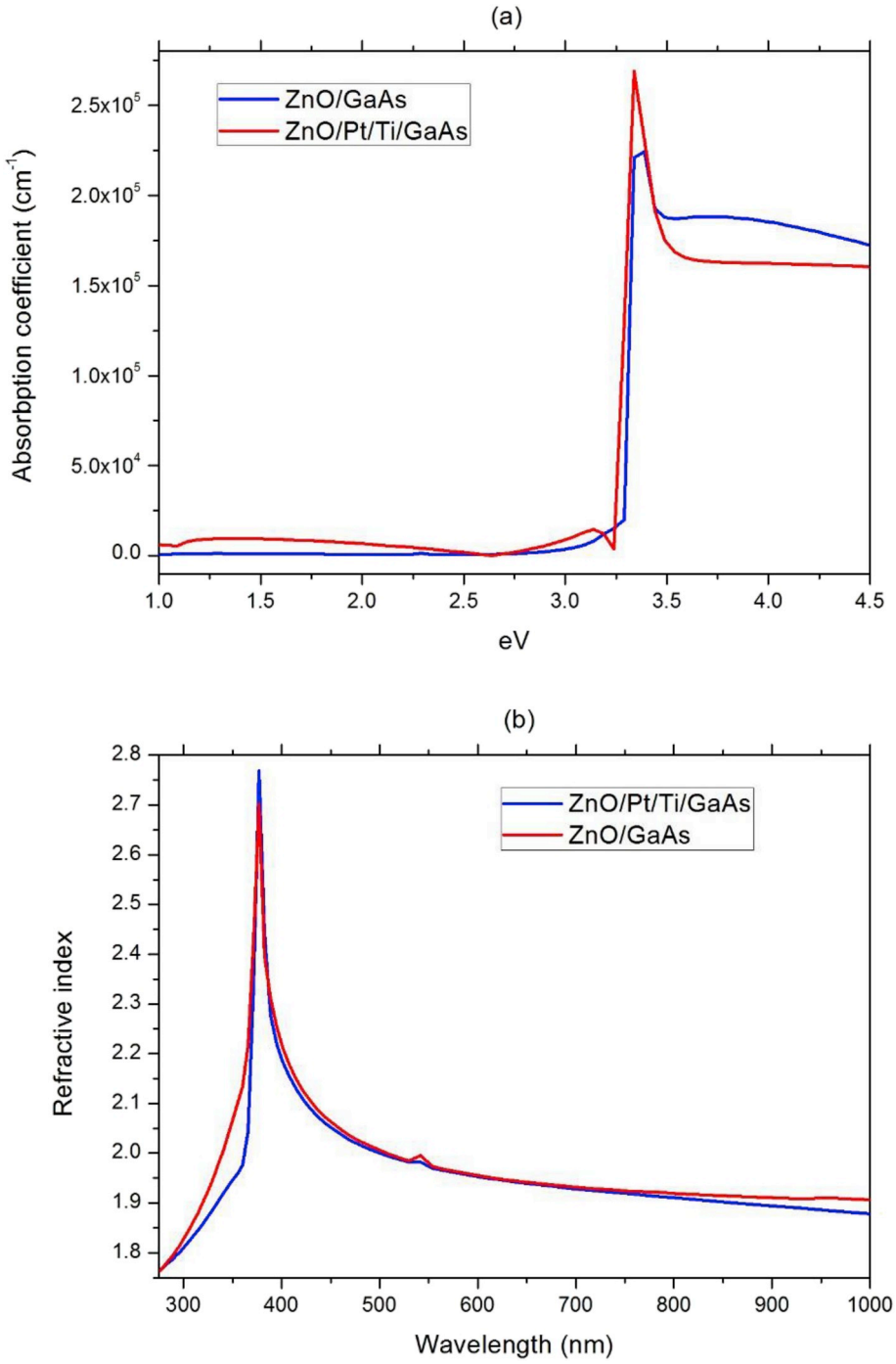

Fig. 5. (a) Absorption coefficient, α and (b) Refractive index, n estimated from the fitting model for ZnO films deposited on GaAs (100) with and without Pt-based buffer layers.

GaAs (100) with and without the Pt/Ti buffer layer shows two main phenomena: the first one is the oxidation of Ti layer during the ZnO deposition, which manifested by the presence/profiles of its oxides (TiO, and TiO_2). The oxidation of these layers was expected since ZnO films were grown using sputtering technique at high oxygen partial pressure. The second is the diffusion of some elements towards the ZnO film. Based on the deposition conditions used for the buffer layer, the thickness of Pt is expected to be 150 nm and that of Ti is expected to be 15 nm. However, the depth profiles of the ZnO/Pt/Ti/GaAs structure (Fig. 4c) show that Ti oxides were found across all the Pt thickness, while it was supposed to be at Pt/GaAs interface. In addition, it was observed that ZnO tends to slightly diffuse to the Pt layer as well. Moreover, Ga ions presented very strong signal, then the signal decrease at the interface was delayed with respect to other detected species. It was clearly obvious that Ga ions diffused to the Pt layer and stopped at the ZnO interface.

The behavior of the different elements could be explained as follows: since the deposition of the ZnO films is carried out at a temperature of 350 °C, Ti has diffused into Pt attracted by the oxygen potential on the surface. As for Ga ion, which tends to diffuse at room temperature in GaAs [59,60], its diffusion stopped at the ZnO interface. However, Ga diffused easily through Ti and Pt layers.

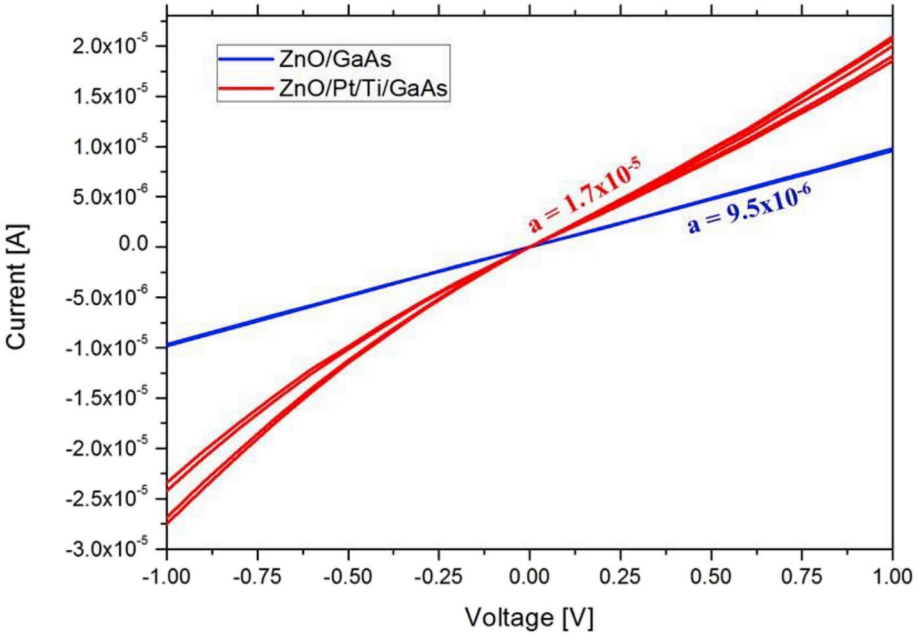

Fig. 6. I–V characteristic of ZnO/GaAs and ZnO/Pt/Ti/GaAs devices.

3.4. Thickness, bandgap and refractive index

The thicknesses of the films were estimated from the ellipsometric data, which allowed to determine the interfaces, and to predict at which depth each element should be located. Hence, the thicknesses of the films were determined at 758 ± 23 nm on Pt/Ti/GaAs and 611 ± 19 nm in the case of direct deposition on GaAs substrates.

The bandgaps of ZnO films deposited on GaAs (100) with and without the buffer layer were within 3.34 and 3.39 eV (Fig. 5a). The measured values were very close to the bandgap of ZnO single crystal (3.33 eV) [61]. The minor difference observed can originate from the stress effect on the films as measured by Raman and XRD.

The refractive index of the films (Fig. 5b), as a function of the wavelength, was also in a reasonable agreement with literature (close to 1.9 below 450 nm) [62]. Some minor difference can be observed in the intensity of the excitonic peak and in the visible absorption of ZnO. These differences may originate from intrinsic defect (oxygen vacancies) or ionic diffusion from the substrate, as observed by SIMS.

3.5. I–V characteristic

The I(V) characteristics were done by doing hysteresis loops from 0 V to 5 V, then from 5 V to −5 V and finally from −5 V to 5 V. The measurements made on ZnO/GaAs and ZnO/Pt/Ti/GaAs are presented in Fig. 6. The conductivity of each device was calculated using the following equation:

$$\kappa = G \times K \quad (8)$$

Where G is the conductance defined as the inverse of the resistance ($G = \frac{1}{a}$, where a is the slope of the I(V) curve in the [-1 V; 1 V] region), and K is proportional to the ratio of the inter-electrode distance (200 μm) to the electrodes surface (3.6×3.6 mm^2).

In the case of the direct deposition of ZnO on undoped GaAs substrate, the I(V) characteristic is linear, indicating an ohmic contact, with a conductivity of 9.5×10^{-6} S/cm. Similarly, for films deposited on Pt/Ti buffer layer, the I(V) characteristic is quasi-linear with a higher conductivity of 1.7×10^{-5} S/cm. The obtained values of current ($\sim 10^{-5}$ A) in the voltage range [-1 V; 1 V] are in reasonable agreement with Fabricius et al. [63]. Some minor hysteresis was also observed in the case of ZnO/Pt/Ti/GaAs, which could originate from charge injection (memristive effect).

4. Discussion

The structural characterization of the ZnO films deposited on the Pt/Ti buffer layer showed better texture and lower residual stress than the films deposited directly on GaAs. Indeed, the films grown with a low deposition rate (2.77 nm/min) and a medium temperature (350 °C) were of higher crystalline quality (FWHM ~ 1.4°) compared to literature (FWHM ~ 3.9°) [44]. In parallel, the morphological characterization showed a better homogeneity, texture and organization of grains in presence of Pt (Rms: 17.9 ± 2.1 nm with Pt vs. 26.5 ± 1.8 without Pt). This indicates that the proposed buffer layer promotes the growth of ZnO films on GaAs with higher crystalline quality. On the other hand, ZnO films grown of fairly good quality were obtained on GaAs (100) with respect to the other tested cuts. In addition to this result, the possibility of micromachining resonant GaAs membranes in this particular cut using chemical wet etching, has motivated us to select GaAs (100) for the development of acoustic wave sensors.

For this application, the transducer requires low conductivity at low voltages. The electrical measurements showed quasi-linear I(V) characteristics for ZnO films grown directly on GaAs and on Pt/Ti/GaAs. The latter presented the lowest conductivity, indicating that the buffer layer can improve not only the structure of the ZnO films, but also the device performance.

However, SIMS analysis revealed a diffusion of Ti and Ga into the Pt layer, which is reasonably in agreement with the literature regarding the problems of diffusion and oxidation of Ti above and below Pt [64–66]. Otherwise, ellipsometric measurements showed that the inter-diffusion in the buffer layer did not affect the bandgap nor the refractive index of ZnO. Nevertheless, the consequences on the overall performances of the sensor would be of concern if Pt was used as a bottom electrode, since it would affect the electrical properties, the durability and the drift over time of the device. Indeed, the diffusion phenomena must be avoided; otherwise, the conductivity of the interface would vary over time and tend to make ZnO film conducting. As ZnO is the material exciting the resonant structure, the piezoelectric performance would be extremely affected if the films were no longer dielectric. Hence, although the piezoelectric layer is of better quality with the Pt/Ti buffer

layer, the inter-diffusion does not make it possible to have a stable device over time. Therefore, further optimization of the interface layer between Pt and GaAs has to be considered to stop the diffusion. This problem could be addressed in the future, by adjusting the deposition temperature, or by adding an extra diffusion barrier at the Pt/GaAs interface, such as TiO_2, which has shown superior stability in the literature [67].

5. Conclusion

Piezoelectric ZnO films were deposited on semi-insulating GaAs substrates using reactive radio frequency magnetron sputtering, for enhancing the piezoelectric performances of a GaAs-based acoustic wave sensor. The effect of the crystalline orientation of the substrate on the films properties was studied, and GaAs (100) was selected for promoting the growth of well-textured ZnO films. The use of a Pt layer was investigated, using Ti buffer layer. The XRD and AFM measurements confirmed that this buffer layer improves the crystalline and structural quality of the films, in terms of texture, stress and roughness, but it promotes the diffusion of Ga and Ti. The characterization of the bandgap and refractive index of the films confirmed that this diffusion did not affect these properties of ZnO. Finally, the lowest conductivity, required for the functioning of an acoustic wave transducer, was determined for the ZnO/Pt/Ti/GaAs structure. This result proves the potential of the proposed buffer layer to promote the growth of high quality ZnO films on GaAs and to provide the electrical contact required for acoustic waves transduction.

Declaration of competing interest

None.

CRediT authorship contribution statement

Juliana Chawich: Investigation, Writing - original draft. **Sabina Kuprenaite:** Investigation, Resources. **Samuel Margueron:** Writing - review & editing. **Pascal Boulet:** Resources. **Jan J. Dubowski:** Supervision, Project administration. **Céline Elie-Caille:** Supervision, Writing - review & editing. **Thérèse Leblois:** Supervision, Funding acquisition, Project administration.

Acknowledgements

Funding for this research was provided by Région de Franche-Comté (France), and by the EUR EIPHI program (Contract "ANR-16-CE24-0002-011"). This work was partly supported by the French RENATECH network and its FEMTO-ST technological facility. The assistance of Josianne Lefebvre (École Polytechnique Montréal) in collecting the SIMS results is greatly appreciated. The authors thank Stefania Oliveri, Benoît Le Roy de Boiseaumarié and Daniel Guneysu from FEMTO-ST Institute (France) for providing technical assistance to the project.

References

[1] K. Hjort, J. Soderkvist, J.-A. Schweitz, Gallium arsenide as a mechanical material, J. Micromech. Microeng. 4 (1994) 1–13, https://doi.org/10.1088/0960-1317/4/1/001.
[2] C.R. Tellier, G. Huve, T.G. Leblois, Micromachining of GaAs structures with an acidic hydrogen peroxide solution, Sens. Actuators Phys. 127 (2006) 179–193, https://doi.org/10.1016/j.sna.2005.11.012.
[3] A. Bienaime, C. Elie-Caille, T. Leblois, Micro structuration of GaAs surface by wet etching: towards a specific surface behavior, J. Nanosci. Nanotechnol. 12 (2012) 6855–6863, https://doi.org/10.1166/jnn.2012.4557.
[4] J. Soderkvist, K. Hjort, The piezoelectric effect of GaAs used for resonators and resonant sensors, J. Micromech. Microeng. 4 (1994) 28–34, https://doi.org/10.1088/0960-1317/4/1/004.
[5] V. Lacour, K. Moumanis, W.M. Hassen, C. Elie-Caille, T. Leblois, J.J. Dubowski, Formation kinetics of mixed self-assembled monolayers of alkanethiols on GaAs (100), Langmuir (2017), https://doi.org/10.1021/acs.langmuir.7b00929.
[6] V. Lacour, C. Elie-Caille, T. Leblois, J.J. Dubowski, Regeneration of a thiolated and antibody functionalized GaAs (001) surface using wet chemical processes, Biointerphases 11 (2016), https://doi.org/10.1116/1.4942878, 019302.
[7] A. Bienaime, T. Leblois, N. Gremaud, M.-J. Chaudon, M. Osta, D. Pecqueur, P. Ducoroy, C. Elie-Caille, Influence of a thiolate chemical layer on GaAs (100) biofunctionalization: an original approach coupling atomic force microscopy and mass spectrometry methods, Materials 6 (2013) 4946–4966, https://doi.org/10.3390/ma6114946.
[8] J.J. Dubowski, O. Voznyy, G.M. Marshall, Molecular self-assembly and passivation of GaAs (001) with alkanethiol monolayers: a view towards bio-functionalization, Appl. Surf. Sci. 256 (2010) 5714–5721, https://doi.org/10.1016/j.apsusc.2010.03.090.
[9] A. Bienaime, L. Liu, C. Elie-Caille, T. Leblois, Design and microfabrication of a lateral excited gallium arsenide biosensor, Eur. Phys. J. Appl. Phys. 57 (2012) 21003, https://doi.org/10.1051/epjap/2011110111.
[10] V. Duplan, Y. Miron, E. Frost, M. Grandbois, J.J. Dubowski, Specific immobilization of influenza A virus on GaAs (001) surface, J. Biomed. Optic. 14 (2009), 054042, https://doi.org/10.1117/1.3251057.
[11] V. Lacour, A. Bienaime, J.-F. Manceau, T. Leblois, J. Dubowski, Design and experimental studies of Gallium Arsenide bulk acoustic wave transducer under lateral field excitation, in: 2014 Eur. Freq. Time Forum EFTF, IEEE, Neuchatel, Switzerland, 2014, pp. 163–166, https://doi.org/10.1109/EFTF.2014.7331454.
[12] J. Chawich, P. Boiteux, C. Elie-caille, T. Leblois, Specificity and sensitivity characterization of a gallium arsenide resonant bio-sensor, in: 2018 IEEE Int. Ultrason. Symp. IUS, IEEE, Kobe, Japan, 2018, pp. 1–4, https://doi.org/10.1109/ULTSYM.2018.8579803.
[13] T. Leblois, V. Lacour, Thermal and conductivity dependence of GaAs based acoustic biosensors, in: 2016 IEEE Int. Ultrason. Symp. IUS, IEEE, Tours, France, 2016, pp. 1–4, https://doi.org/10.1109/ULTSYM.2016.7728852.
[14] E.A. Cerda-Méndez, D. Krizhanovskii, K. Biermann, R. Hey, P.V. Santos, M. S. Skolnick, Effects of the piezoelectric field on the modulation of exciton–polaritons by surface acoustic waves, Superlattice. Microst. 49 (2011) 233–240, https://doi.org/10.1016/j.spmi.2010.06.006.
[15] S.J. Jiao, P.D. Batista, K. Biermann, R. Hey, P.V. Santos, Electrical detection of ambipolar acoustic carrier transport by surface acoustic waves, J. Appl. Phys. 106 (2009), https://doi.org/10.1063/1.3211861, 053708.
[16] O.D.D. Couto, F. Iikawa, J. Rudolph, R. Hey, P.V. Santos, Anisotropic spin transport in (110) GaAs quantum wells, Phys. Rev. Lett. 98 (2007), https://doi.org/10.1103/PhysRevLett.98.036603.
[17] W.-C. Shih, M.-S. Wu, Growth of ZnO films on GaAs substrates with a SiO_2 buffer layer by RF planar magnetron sputtering for surface acoustic wave applications, J. Cryst. Growth 137 (1994) 319–325, https://doi.org/10.1016/0022-0248(94)90968-7.
[18] Y.Q. Fu, J.K. Luo, X.Y. Du, A.J. Flewitt, Y. Li, G.H. Markx, A.J. Walton, W.I. Milne, Recent developments on ZnO films for acoustic wave based bio-sensing and microfluidic applications: a review, Sensor. Actuator. B Chem. 143 (2010) 606–619, https://doi.org/10.1016/j.snb.2009.10.010.
[19] Ü. Özgür, Y.I. Alivov, C. Liu, A. Teke, M.A. Reshchikov, S. Doğan, V. Avrutin, S.-J. Cho, H. Morkoç, A comprehensive review of ZnO materials and devices, J. Appl. Phys. 98 (2005), https://doi.org/10.1063/1.1992666, 041301.
[20] S. Singh, P. Thiyagarajan, K. Mohan Kant, D. Anita, S. Thirupathiah, N. Rama, B. Tiwari, M. Kottaisamy, M.S. Ramachandra Rao, Structure, microstructure and physical properties of ZnO based materials in various forms: bulk, thin film and nano, J. Phys. Appl. Phys. 40 (2007) 6312–6327, https://doi.org/10.1088/0022-3727/40/20/S15.
[21] Ü. Özgür, D. Hofstetter, H. Morkoç, ZnO devices and applications: a review of current status and future prospects, Proc. IEEE 98 (2010) 1255–1268, https://doi.org/10.1109/JPROC.2010.2044550.
[22] C. Klingshirn, ZnO: from basics towards applications, Phys. Status Solidi B 244 (2007) 3027–3073, https://doi.org/10.1002/pssb.200743072.
[23] D.-S. Liu, C.-Y. Wu, C.-S. Sheu, F.-C. Tsai, C.-H. Li, The preparation of piezoelectric ZnO films by RF magnetron sputtering for layered surface acoustic wave device applications, Jpn. J. Appl. Phys. 45 (2006) 3531–3536, https://doi.org/10.1143/JJAP.45.3531.
[24] L. Mai, V.-S. Pham, G. Yoon, ZnO-based film bulk acoustic resonator devices on a specially designed Bragg reflector, Appl. Phys. A 95 (2009) 667–671, https://doi.org/10.1007/s00339-009-5142-1.
[25] S. Krishnamoorthy, A.A. Iliadis, Development of high frequency ZnO/SiO_2/Si Love mode surface acoustic wave devices, Solid State Electron. 50 (2006) 1113–1118, https://doi.org/10.1016/j.sse.2006.04.033.
[26] E. Praveen, S. Murugan, K. Jayakumar, Nano ZnO embedded in Chitosan matrix for vibration sensor application, Rome, Italy, in: NANOFORUM 2014, 2015, https://doi.org/10.1063/1.4917673, 050032.
[27] Y. Yoshino, Piezoelectric thin films and their applications for electronics, J. Phys. Appl. Phys. 105 (2009), https://doi.org/10.1063/1.3072691, 061623.
[28] C. Jagadish, S.J. Pearton, Zinc Oxide Bulk, Thin Films and Nanostructures: Processing, Properties, and Applications, first ed., Elsevier, 2006.
[29] X.Y. Du, Y.Q. Fu, J.K. Luo, A.J. Flewitt, W.I. Milne, Microfluidic pumps employing surface acoustic waves generated in ZnO thin films, J. Phys. Appl. Phys. 105 (2009), https://doi.org/10.1063/1.3068326, 024508.
[30] A. Hongsingthong, I. Afdi Yunaz, S. Miyajima, M. Konagai, Preparation of ZnO thin films using MOCVD technique with D_2O/H_2O gas mixture for use as TCO in silicon-based thin film solar cells, Sol. Energy Mater. Sol. Cells 95 (2011) 171–174, https://doi.org/10.1016/j.solmat.2010.04.025.
[31] L. Bentes, R. Ayouchi, C. Santos, R. Schwarz, P. Sanguino, O. Conde, M. Peres, T. Monteiro, O. Teodoro, ZnO films grown by laser ablation with and without

oxygen CVD, Superlattice. Microst. 42 (2007) 152–157, https://doi.org/10.1016/j.spmi.2007.04.049.
[32] N. Lehraki, M.S. Aida, S. Abed, N. Attaf, A. Attaf, M. Poulain, ZnO thin films deposition by spray pyrolysis: influence of precursor solution properties, Curr. Appl. Phys. 12 (2012) 1283–1287, https://doi.org/10.1016/j.cap.2012.03.012.
[33] R. Ondo-Ndong, G. Ferblantier, M. Al Kalfioui, A. Boyer, A. Foucaran, Properties of RF magnetron sputtered zinc oxide thin films, J. Cryst. Growth 255 (2003) 130–135, https://doi.org/10.1016/S0022-0248(03)01243-0.
[34] W.L. Dang, Y.Q. Fu, J.K. Luo, A.J. Flewitt, W.I. Milne, Deposition and characterization of sputtered ZnO films, Superlattice. Microst. 42 (2007) 89–93, https://doi.org/10.1016/j.spmi.2007.04.081.
[35] J. Molarius, J. Kaitila, T. Pensala, M. Ylilammi, Piezoelectric ZnO films by rf sputtering, J. Mater. Sci. Mater. Electron. 14 (2003) 431–435, https://doi.org/10.1023/A:1023929524641.
[36] S. Bensmaine, L. Le Brizoual, O. Elmazria, J.J. Fundenberger, B. Benyoucef, Deposition of ZnO inclined c-axis on silicon and diamond by r.f. magnetron sputtering, Phys. Status Solidi 204 (2007) 3091–3095, https://doi.org/10.1002/pssa.200776322.
[37] P. Wang, H. Du, S. Shen, M. Zhang, B. Liu, Deposition, characterization and optimization of zinc oxide thin film for piezoelectric cantilevers, Appl. Surf. Sci. 258 (2012) 9510–9517, https://doi.org/10.1016/j.apsusc.2012.04.158.
[38] K.B. Sundaram, A. Khan, Characterization and optimization of zinc oxide films by r.f. magnetron sputtering, Thin Solid Films 295 (1997) 87–91, https://doi.org/10.1016/S0040-6090(96)09274-7.
[39] G. Sai Krishna Santosh, H.B. Nemade, Investigation of properties of surface acoustic waves generated by periodically patterned ZnO on silicon substrate, Ultrasonics 59 (2015) 40–44, https://doi.org/10.1016/j.ultras.2015.01.008.
[40] R.S. Gonçalves, P. Barrozo, G.L. Brito, B.C. Viana, F. Cunha, The effect of thickness on optical, structural and growth mechanism of ZnO thin film prepared by magnetron sputtering, Thin Solid Films 661 (2018) 40–45, https://doi.org/10.1016/j.tsf.2018.07.008.
[41] H.K. Kim, M. Mathur, Thermally stable ZnO films deposited on GaAs substrates with a SiO_2 thin buffer layer, Appl. Phys. Lett. 61 (1992) 2524–2526, https://doi.org/10.1063/1.108169.
[42] M. Soylu, A.A. Al-Ghamdi, O.A. Al-Hartomy, F. El-Tantawy, F. Yakuphanoglu, The electrical characterization of ZnO/GaAs heterojunction diode, Phys. E Low-Dimens. Syst. Nanostruct. 64 (2014) 240–245, https://doi.org/10.1016/j.physe.2014.08.001.
[43] J. Jou, M. Han, D. Cheng, Substrate dependent internal stress in sputtered zinc oxide thin films, J. Appl. Phys. 71 (1992) 4333–4336, https://doi.org/10.1063/1.350815.
[44] J. Pedrós, L. García-Gancedo, C.J.B. Ford, C.H.W. Barnes, J.P. Griffiths, G.A. C. Jones, A.J. Flewitt, Guided propagation of surface acoustic waves and piezoelectric field enhancement in ZnO/GaAs systems, J. Appl. Phys. 110 (2011), https://doi.org/10.1063/1.3660215, 103501.
[45] M.K. Ryu, S.H. Lee, M.S. Jang, G.N. Panin, T.W. Kang, Postgrowth annealing effect on structural and optical properties of ZnO films grown on GaAs substrates by the radio frequency magnetron sputtering technique, J. Appl. Phys. 92 (2002) 154–158, https://doi.org/10.1063/1.1483371.
[46] Y.-C. Huang, L.-W. Weng, W.-Y. Uen, S.-M. Lan, Z.-Y. Li, S.-M. Liao, T.-Y. Lin, T.-N. Yang, Annealing effects on the p-type ZnO films fabricated on GaAs substrate by atmospheric pressure metal organic chemical vapor deposition, J. Alloys Compd. 509 (2011) 1980–1983, https://doi.org/10.1016/j.jallcom.2010.10.108.
[47] Y. Kim, W.D. Hunt, F.S. Hickernell, R.J. Higgins, Surface acoustic wave properties of ZnO films on {001}-cut<110>-propagating GaAs substrates, J. Appl. Phys. 75 (1994) 7299–7303, https://doi.org/10.1063/1.356639.
[48] A.B.M.A. Ashrafi, A. Ueta, A. Avramescu, H. Kumano, I. Suemune, Y.-W. Ok, T.-Y. Seong, Growth and characterization of hypothetical zinc-blende ZnO films on GaAs(001) substrates with ZnS buffer layers, Appl. Phys. Lett. 76 (2000) 550–552, https://doi.org/10.1063/1.125851.
[49] K. Zhao, L. Ye, M.C. Tamargo, A. Shen, Plasma-assisted MBE growth of ZnO on GaAs substrate with a ZnSe buffer layer, Phys. Status Solidi C 9 (2012) 1809–1812, https://doi.org/10.1002/pssc.201100613.
[50] T.C. Damen, S.P.S. Porto, B. Tell, Raman effect in zinc oxide, Phys. Rev. 142 (1966) 570, https://doi.org/10.1103/PhysRev.142.570.
[51] Y. Zhang, H. Jia, R. Wang, C. Chen, X. Luo, D. Yu, C. Lee, Low-temperature growth and Raman scattering study of vertically aligned ZnO nanowires on Si substrate, Appl. Phys. Lett. 83 (2003) 4631–4633, https://doi.org/10.1063/1.1630849.
[52] I. Zardo, S. Conesa-Boj, F. Peiro, J.R. Morante, J. Arbiol, E. Uccelli, G. Abstreiter, A. Fontcuberta i Morral, Raman spectroscopy of wurtzite and zinc-blende GaAs nanowires: polarization dependence, selection rules, and strain effects, Phys. Rev. B 80 (2009), https://doi.org/10.1103/PhysRevB.80.245324.
[53] K. Sato, S. Adachi, Optical properties of ZnTe, J. Appl. Phys. 73 (1993) 926–931, https://doi.org/10.1063/1.353305.
[54] S. Kuprenaite, S. Margueron, M. Raschetti, C. Millon, T. Baron, W. Daniau, S. Ballandras, B. Gautier, D. Albertini, P. Boulet, A. Bartasyte, Effect of $LiNbO_3$ polarity on the structural, optical and acoustic properties of epitaxial ZnO and $Mg_x Zn_{1-x} O$ films, J. Phys. Appl. Phys. 51 (2018), https://doi.org/10.1088/1361-6463/aadcce, 484003.
[55] A. Bartasyte, V. Plausinaitiene, A. Abrutis, T. Murauskas, P. Boulet, S. Margueron, J. Gleize, S. Robert, V. Kubilius, Z. Saltyte, Residual stresses and clamped thermal expansion in $LiNbO_3$ and $LiTaO_3$ thin films, Appl. Phys. Lett. 101 (2012) 122902, https://doi.org/10.1063/1.4752448.
[56] T.B. Bateman, Elastic moduli of single-crystal zinc oxide, J. Appl. Phys. 33 (1962) 3309–3312, https://doi.org/10.1063/1.1931160.
[57] H.F. Pang, G.A. Zhang, Y.L. Tang, Y.Q. Fu, L.P. Wang, X.T. Zu, F. Placido, Substrate-tilt angle effect on structural and optical properties of sputtered ZnO film, Appl. Surf. Sci. 259 (2012) 747–753, https://doi.org/10.1016/j.apsusc.2012.07.114.
[58] A. Bartasyte, S. Margueron, J. Kreisel, P. Bourson, O. Chaix-Pluchery, L. Rapenne-Homand, J. Santiso, C. Jimenez, A. Abrutis, F. Weiss, M.D. Fontana, Residual stress estimation in ferroelectric $PbTiO_3$ thin films by Raman spectroscopy, Phys. Rev. B 79 (2009), https://doi.org/10.1103/PhysRevB.79.104104.
[59] D.J. Schroeder, G.D. Berry, A.A. Rockett, Gallium diffusion and diffusivity in $CuInSe_2$ epitaxial layers, Appl. Phys. Lett. 69 (1996) 4068–4070, https://doi.org/10.1063/1.117820.
[60] T.Y. Tan, S. Yu, U. Gösele, Determination of vacancy and self-interstitial contributions to gallium self-diffusion in GaAs, J. Appl. Phys. 70 (1991) 4823–4826, https://doi.org/10.1063/1.349048.
[61] V. Srikant, D.R. Clarke, On the optical band gap of zinc oxide, J. Appl. Phys. 83 (1998) 5447–5451, https://doi.org/10.1063/1.367375.
[62] W.L. Bond, Measurement of the refractive indices of several crystals, J. Appl. Phys. 36 (1965) 1674–1677, https://doi.org/10.1063/1.1703106.
[63] H. Fabricius, T. Skettrup, P. Bisgaard, Ultraviolet detectors in thin sputtered ZnO films, Appl. Optic. 25 (1986) 2764, https://doi.org/10.1364/AO.25.002764.
[64] G.R. Fox, S. Trolier-McKinstry, S.B. Krupanidhi, L.M. Casas, Pt/Ti/SiO_2/Si substrates, J. Mater. Res. 10 (1995) 1508–1515, https://doi.org/10.1557/JMR.1995.1508.
[65] K.H. Park, C.Y. Kim, Y.W. Jeong, H.J. Kwon, K.Y. Kim, J.S. Lee, S.T. Kim, Microstructures and interdiffusions of Pt/Ti electrodes with respect to annealing in the oxygen ambient, J. Mater. Res. 10 (1995) 1790–1794, https://doi.org/10.1557/JMR.1995.1790.
[66] T. Maeder, L. Sagalowicz, P. Muralt, Stabilized platinum electrodes for ferroelectric film deposition using Ti, Ta and Zr adhesion layers, Jpn. J. Appl. Phys. 37 (1998) 2007–2012, https://doi.org/10.1143/JJAP.37.2007.
[67] A.J. Fox, B. Drawl, G.R. Fox, B.J. Gibbons, S. Trolier-McKinstry, Control of crystallographic texture and surface morphology of Pt/TiO_2 templates for enhanced PZT thin film texture, IEEE Trans. Ultrason. Ferroelectrics Freq. Contr. 62 (2015) 56–61, https://doi.org/10.1109/TUFFC.2014.006671.